

A Compact Setup of Saturated Absorption Spectroscopy for Diode Laser Frequency Stabilization *

ZHANG Xian(章显), HUANG Kai-Kai(黄凯凯)**, XU Hao(徐浩), XU Zhou-Xiang(徐周翔),
LI Nan(李楠), LU Xuan-Hui(陆璇辉)

Institute of Optics, Department of Physics, Zhejiang University, Hangzhou 310027

(Received 13 March 2012)

A novel setup of saturated absorption spectroscopy (SAS) is presented. It is based on laser reflections at surfaces of a sample vapor cell. It only needs one cell and one photodiode and is more compact than conventional setups of SAS. Its spectrum is similar to a conventional SAS. The frequency stabilization performance of an external-cavity diode laser with this setup is investigated. A frequency stability of 1.1×10^{-11} is achieved at an averaging time of 60 s in the Allen variance measurements.

PACS: 42.62.Fi, 42.60.Lh, 42.79.Fm

DOI: 10.1088/0256-307X/29/7/074206

In the past decades, saturated absorption spectroscopy (SAS)^[1–3] has been used in laser frequency stabilization and atomic physics, especially in laser cooling and trapping,^[4–6] due to the fact that SAS eliminates Doppler broadening so that a laser can be frequency-stabilized on a hyperfine transition with SAS. Also, SAS plays an important role in other laser frequency stabilization techniques such as polarization spectroscopy,^[7,8] and heterodyne frequency stabilization with magnetically, acoustically or electronically induced modulation.^[9–11]

Though the SAS techniques have been used for a long time, the optical structures of SAS devices remain almost unchanged. For applications to such as portable atomic clocks and atomic interferometers,^[12] the conventional structure of SAS is now facing a challenge of miniaturization. Particularly for some applications such as in satellite-based equipments,^[13] the payloads always need decreasing weight and reducing size. In general, an experimental setup of conventional SAS consists of a laser, several total reflectors, a polarization beam splitter (PBS) or beam splitter (BS), a sample vapor cell, and a photodetector (PD). They are usually arranged in a layout of a triangle^[14] or in a quasi-straight line.^[15] These experimental setups involve quite a lot optical elements that will occupy room. Furthermore, optical properties of these optical elements may be affected by ambient temperature or air turbulence fluidity, which will affect the spectrum properties. Therefore, optimizing of SAS is helpful in actual applications. In this Letter, we present a setup of SAS based on laser reflections at vapor cell surfaces (SASRS) whose configuration is more compact than conventional SAS, and applies SASRS in laser frequency stabilizations.

The schematic setup and experimental picture of the SASRS are shown in Fig. 1. When an incident laser beam passes through the vapor cell, it will be reflected by the front and rear surfaces of the vapor cell. In this case, we treat the beams reflected by the external face and the inner face of the glass wall as the same beam, since the glass wall of the cell is very thin. The beam reflected by the rear surface acts as the probe beam, while the incident beam acts as the pump beam. These two beams overlap in the cell. The probe beam then is partially reflected by the front surface and propagates to the PD. Since the SASRS uses the partial reflection of the vapor cell, glass blocks and mirrors in conventional SAS setups can be removed in SASRS, the laser frequency stabilization system can be more compact and portable.

In our experiment, a 780 nm external-cavity diode laser (ECDL) in a littrow configuration was used. The ISO in the layout is an optical isolator (OFR IO-5-780-PBS). The PBS has an extinction ratio up to ~ 30 dB at 780 nm. The sample vapor in the cell is rubidium isotopes ^{85}Rb and ^{87}Rb . The Rb cell is made of K9 glass, and the vapor pressure in it is 6×10^{-5} Pa at 25°C. The temperature of the Rb cell can be controlled by a heating tape to obtain good properties of the spectrum. The laser beam with a waist of 2 mm has a free running linewidth of 300 kHz. After the beam is split by the PBS, most of its power is used for applied experiments, for example, cooling beams in laser cooling experiments, while a little part of the power is used for SASRS. The probe beam was linearly polarized parallel to the pump beam polarization. The surface reflectivity of the cell at 780 nm is 6.4% according to measurements. In other words, the intensity ratio of the probe beam and pump beam is 6.4%. This

*Supported by the National Basic Research Program of China under Grant No 2012CB921602, and the National Natural Science Foundation of China under Grant Nos 10874012 and 10974177, and the Program of International Science and Technology Cooperation of China under Grant No 2010DFA04690.

**Correspondence author. Email: huangkaikai@zju.edu.cn

© 2012 Chinese Physical Society and IOP Publishing Ltd

value meets the requirement of saturated absorption. Typically, the pump beam intensity is 20 mW/cm^2 , and the probe beam 1.3 mW/cm^2 . Hence the intensity of the probe beam actually detected by the PD is $80 \mu\text{W/cm}^2$. To avoid the pump beam being detected by PD, the pump beam and the probe beam are actually separated by a tiny angle of about 40 mrad by tilting the cell 20 mrad from the laser axis, while the overlap of the beams in the cell still satisfies experimental requests. The PD is a Hamamatsu S5821-01. Its signal is amplified with a gain factor of 100 by a homemade amplifier to satisfy the requirement of frequency stabilization. We use a lock-in regulator (Top-tica LIR 110) to internally modulate the piezoelectric ceramic transformer (PZT) and current of the ECDL, and to lock it on a transition line between two certain hyperfine energy levels. Also, the laser frequency can be tuned over hyperfine transitions by changing the PZT voltage. In practice, the ECDL, half wavelength plate (HWP), PBS, Rb cell and PD are all integrated on a breadboard which is about 30 cm long and 20 cm wide. The size of the optical bench will be further reduced if state-of-the-art bonding techniques are used.

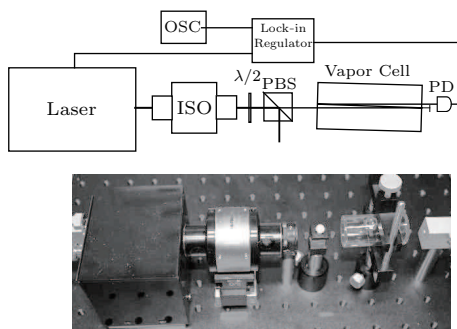


Fig. 1. Schematic setup and experimental picture of the SASRS. OSC: oscilloscope.

The spectrum properties of the SASRS without any PZT or current modulation are investigated. As shown in Fig. 2, the SASRS provides a spectrum (solid) on which the peaks reveal the $F = 2 \rightarrow F'$ hyperfine transitions of ^{87}Rb D_2 lines. The frequencies at these peaks are options for cooling laser beams in a magneto-optical trap (MOT) of ^{87}Rb . In our experiments we choose the crossover peak of the $F = 2 \rightarrow F' = 2$ and $F = 2 \rightarrow F' = 3$ transitions (CO 2-23 for short, which denotes the crossover transition of $F = 2 \rightarrow F' = 2$ and $F = 2 \rightarrow F' = 3$), since its error signal is the largest and the most suitable one for identifying and laser frequency stabilization. Also, Fig. 2 is a comparison between the SASRS (solid) and the conventional SAS (dashed). The temperature of the Rb cell in these two cases is controlled at 50°C . The conventional one is carried out when probe beam intensity is 0.2 mW/cm^2 and pump beam intensity 2 mW/cm^2 . As is known, the theoretical relative amplitudes of these peaks are independent of the pump and probe beam

intensities:^[16]

$$I_{ij} = |\mu_i|^2 \cdot |\mu_j|^2 \cdot (-\delta_{i,sp} + |\mu_{sp}|^2/\Gamma_F), \quad (1)$$

where I_{ij} is the intensity of the spectrum, $|\mu_i|^2$, $|\mu_j|^2$ and $|\mu_{sp}|^2$ are the probabilities of transitions induced by the pump beam, the probe beam and the spontaneous emission respectively. The Γ_F is the total transition probability of each hyperfine level F , and $\delta_{i,sp}$ is Kronecker's δ symbol. If i and sp denotes the same transition, $\delta_{i,sp}$ becomes unity, otherwise $\delta_{i,sp} = 0$. Though the absolute intensities of the peaks depend on the intensities of the pump beam and probe beam, the relative intensities are invariable with them. However, the absolute intensity of the spectrum is affected by the Doppler broadening factor which is affected by the beam intensity. As a result, the Doppler broadened envelope of the solid spectrum in Fig. 2 is deeper than that of the dashed one. This fact can be explained as follows: (i) the cell surface reflectivity is rather small so that the pumping intensity of the SASRS is larger than that of the conventional SAS; (ii) the probing-pumping intensity ratios of these two SAS setups are different; and (iii) in the SASRS, the probe beam finally detected by PD is double absorbed as it passes through the cell twice. The point (iii) is an essential difference between SASRS and conventional SAS. This difference is worth investigating further, especially when various polarizations and magnetic fields are introduced.

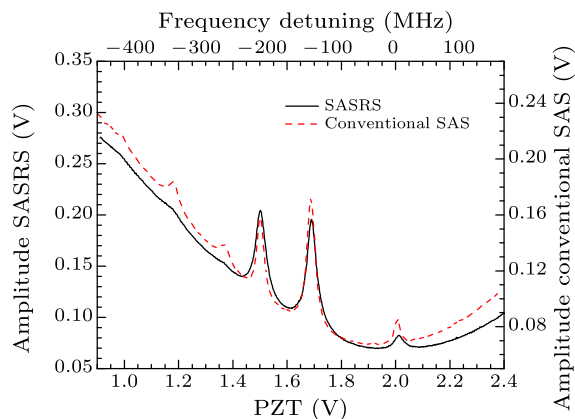


Fig. 2. A comparison between the SASRS (solid) and the conventional SAS (dashed). The top x axis is the frequency detuning where the reference point 0 MHz is the transition line $F = 2 \rightarrow F' = 3$. The temperature of the Rb cell is 50°C .

In this work, as a spectrum for laser frequency stabilization, the most important properties are the FWHMs of the peaks and the signal-to-noise ratios (SNRs) of the corresponding error signals, since these parameters correlate to the stability of laser frequency stabilization. For the crossover transition CO 2-23, the FWHMs of these two spectra are identical according to Fig. 2. We also quantitatively measured the

FWHM of CO 2-23 with beat frequency. Its value is 6 MHz, which is consistent with the natural linewidth of ^{87}Rb

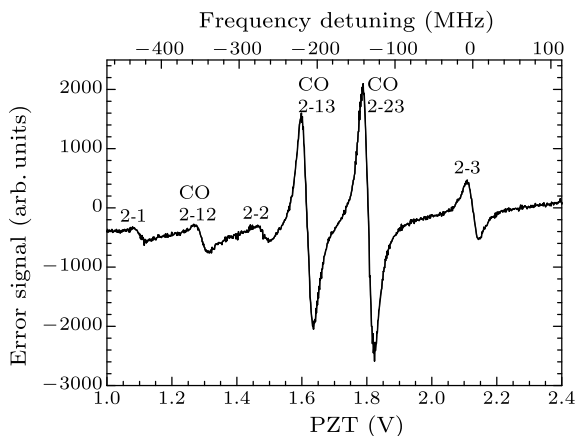


Fig. 3. Error signals of the ^{87}Rb D2 lines of SASRS with internal modulation (the mark CO in this figure stands for crossover transitions). The top x axis is the frequency detuning where the reference point 0 MHz is the transition line $F = 2 \rightarrow F' = 3$. The temperature of the Rb cell is 50°C .

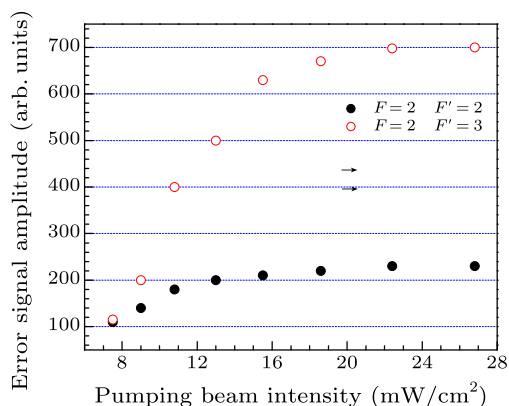


Fig. 4. Dependence of the error signal amplitude on the pump beam intensity. The temperature of the Rb cell is 50°C . The closed circles denote the data of the $F = 2 \rightarrow F' = 2$ component, and the open circles denote the data of the $F = 2 \rightarrow F' = 3$ component.

Figure 3 shows the error signals corresponding to the $F = 2 \rightarrow F'$ hyperfine transitions of ^{87}Rb D_2 lines of SASRS using internal modulation, with the temperature of the Rb cell controlled at 50°C , where the saturation spectrum has larger amplitude and the same FWHM compared with those at 20°C . The modulation frequency is 85 kHz, with amplitude of 0.01 V. The saturation spectrum signal is ac coupled into the lock-in regulator and the error signal here is the first-order derivation of the input spectrum signal, so the Doppler broadened envelope is eliminated. Each zero-crossing on slopes of the error signal corresponds to a peak on the SAS spectrum. The largest slope that denotes the crossover peak CO 2-23 is the error signal used for laser frequency stabilization in this work.

The dependence of the error signals of sub-Doppler resonances on the pumping intensity is investigated. Figure 4 shows the error signal amplitude against the pump beam intensity. Both the $F = 2 \rightarrow F' = 2$ and $F = 2 \rightarrow F' = 3$ components increase from an identical amplitude with the pump beam intensity, while the $F = 2 \rightarrow F' = 3$ component increases to amplitudes much higher than that for the $F = 2 \rightarrow F' = 2$ component. This fact is not expected by formula (1), and is caused by the changes of the Doppler broadening envelope as the optical pumping strengthens with the increasing pumping beam intensity. For the crossover transition CO 2-23, when the pump beam intensity is $20\text{ mW}/\text{cm}^2$, where both the $F = 2 \rightarrow F' = 2$ and $F = 2 \rightarrow F' = 3$ components reach higher amplitudes, the SNR of the error signal for crossover transition CO 2-23 is typically 150, obtained by measuring the Fourier spectra of the error signal.

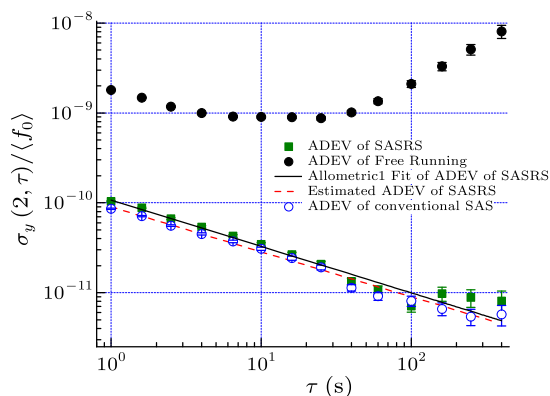


Fig. 5. Allan standard deviation of two ECDLs at free running (closed circle), internal-modulation locked with SASRS (square), and internal-modulation locked with conventional SAS (open circle), respectively. Sampling time $\tau_0 = 0.5\text{ s}$. The solid straight line is the allometric-1 (power law) fit of the ADEV, and the dashed line is an estimated ADEV based on SNR of the error signal.

We measured the frequency stability at the locked peak CO 2-23 (384227.77 GHz) with Allan variance.^[17] Using a universal counter (Agilent 53131 A), this experiment was carried out by recording the frequency beat notes of two lasers frequency-stabilized with SASRS and conventional SAS, both with the same PID parameters. Figure 5 shows the relative Allan deviation (ADEV) of two ECDLs at free running (circle), two ECDLs frequency-stabilized with internal-modulation of SASRS (square), and with conventional SAS (hollow circle), respectively. When two ECDLs are frequency-locked with SASRS, the ADEV is 1.0×10^{-10} at 1 s and 1.1×10^{-11} at 60 s. Due to the finite sample number m , their uncertainties are 2.7×10^{-13} and 5.8×10^{-13} , respectively, according to the relationship

$$\delta \sim \sigma_y(\tau) / \sqrt{m}. \quad (2)$$

During $\tau = 1\text{--}100\text{ s}$, in the log-log plot, the curve of

Allan deviation goes down linearly with the increasing τ . At $\tau > 100$ s, the ADEV has a small fluctuation, but it still maintains below 1×10^{-11} .

The slope of the ADEV of SASRS is $\mu = -0.51$ according to the Allometric-1 fitting (solid straight line in Fig. 5). Thus the ADEV can be written in a power law:

$$\sigma_y^2(\tau) = a \cdot \tau^{-1}. \quad (3)$$

This means that the major noise of the SASRS spectrum is white noise frequency modulation (WFM),^[17] which is normal for laser stabilizations with internal modulation of SAS and without phase locking. More explicitly, the frequency stability is determined by^[15,18]

$$\sigma_y(\tau) \approx \frac{k\Delta\nu}{\nu_0\sigma_{\text{SNR}}} \cdot \tau^{-1/2}, \quad (4)$$

where $\Delta\nu$ is the linewidth (FWHM) of the hyperfine transition, ν_0 is the laser frequency, and σ_{SNR} is the signal-to-noise ratio of the error signal. The factor k correlates to the steepness of the slope of the corresponding error signal and is around 1 for the first derivative spectrum.^[15] The dashed line in Fig. 5 is an estimated ADEV according to formula (4). The estimated result agrees with the measured ADEV data (square). The fluctuation of the ADEV at $\tau > 100$ s in Fig. 5 is due to the slow changes of the laser parameters and environment perturbation. According to the ADEV of conventional SAS (hollow circles) in Fig. 5, the results also show that the spectrum of the SASRS has comparable stability and SNR against a conventional SAS.

In summary, we have presented a novel compact setup of saturated absorption spectroscopy. It is based on laser reflections at the surfaces of vapor cells (SASRS). Compared with conventional SAS, SASRS

has an advantage with fewer optical elements (actually only one cell and one PD) and smaller size. Due to its compactness and portability, SASRS is especially beneficial to portable systems, such as portable gyroscopes based on atomic interferometry, or satellite-based equipment, etc. We have also studied its spectrum properties that correlate to the quality of laser frequency stabilization. Compared with conventional SAS, SASRS provides a comparable performance of laser stabilization. The relative Allan deviation is below 10^{-10} at averaging time $\tau = 1$ –100 s and reaches the magnitude of 10^{-12} at $\tau = 100$ –400 s.

References

- [1] BENNETT W R Jr 1962 *Phys. Rev.* **126** 580
- [2] Banerjee A and Natarajan V 2003 *Opt. Lett.* **28** 1912
- [3] Duan J, Qi X, Zhou X and Chen X 2011 *Opt. Lett.* **36** 561
- [4] Phillips W D 1997 *Rev. Mod. Phys.* **70** 721
- [5] Metcalf H J and Straten P van der 1999 *Laser Cooling and Trapping* (New York: Springer)
- [6] Cheng H D et al 2009 *Phys. Rev. A* **79** 023407
- [7] Wieman C E and Hänsch T W 1976 *Phys. Rev. Lett.* **36** 1170
- [8] Yin C et al 2011 *Chin. Phys. Lett.* **28** 094204
- [9] Corwin K L, Lu Z T, Hand C F, Epstein R J and Wieman C E 1998 *Appl. Opt.* **37** 3295
- [10] Sukenik C I, Busch H C and Shiddiq M 2002 *Opt. Commun.* **203** 133
- [11] Qi X H et al 2009 *Chin. Phys. Lett.* **26** 044205
- [12] Biedermann G 2007 *PhD Dissertation* (Stanford University)
- [13] Jentsch C, Müller T, Rasel E M and Ertmer W 2004 *Gen. Rel. Grav.* **36** 2197
- [14] Kasevich M A 1992 *PhD Dissertation* (Stanford University)
- [15] Talvitie H, Merimaa M and Ikonen E 1998 *Opt. Commun.* **152** 182
- [16] Nakayama S 1984 *Jpn. J. Appl. Phys.* **23** 879
- [17] Allan D W 1966 *Proc. IEEE* **54** 221
- [18] Fukuda K, Tachikawa M and Kinoshita M 2003 *Appl. Phys. B* **77** 823